ACS APPLIED ENERGY MATERIALS



Article

# Uniform Selenization of Crack-Free Films of Cu(In,Ga)Se2 Nanocrystals

Taylor B Harvey, Franco Bonafe, Ty Updegrave, Vikas Reddy Voggu, Cherrelle Thomas, Sirish Kamarajugadda, Carl Jackson Stolle, Douglas R. Pernik, Jiang Du, and Brian A. Korgel

*ACS Appl. Energy Mater.*, **Just Accepted Manuscript** • DOI: 10.1021/acsaem.8b01800 • Publication Date (Web): 04 Dec 2018

# Uniform Selenization of Crack-Free Films of $Cu(In,Ga)Se_2$ Nanocrystals

Taylor B. Harvey, [†,*] Franco Bonafé, [‡,§] Ty Updegrave,[ǁ] Vikas Reddy Voggu,[ǁ] Cherrelle Thomas,[ǁ] Sirish C. Kamarajugadda,[ǁ] C. Jackson Stolle,[ǁ] Douglas Pernik,[ǁ] Jiang Du,[ǁ] Brian A. Korgel[*,ǁ]

[†]Department of Science and Mathematics, Texas A&M University-Central Texas, Killeen, TX 76549, USA

[‡]Universidad Nacional de Córdoba. Facultad de Ciencias Químicas, Departamento de Química Teórica y Computacional. X5000HUA Córdoba, Argentina

[§]Instituto de Investigaciones en Fisicoquímica de Córdoba, INFIQC (CONICET - Universidad Nacional de Córdoba). X5000HUA Córdoba, Argentina

[ǁ]McKetta Department of Chemical Engineering and Texas Materials Institute, The University of Texas at Austin, Austin, Texas 78712, USA

* Corresponding Authors: tharvey@tamuct.edu; korgel@che.utexas.edu

**Abstract**

Crack-free films of $Cu(In,Ga)Se_2$ (CIGS) nanocrystals were deposited with uniform thickness (>1μm) on Mo-coated glass substrates using an ink-based, automated ultrasonic spray process, then selenized and incorporated into photovoltaic devices (PVs). The device performance depended strongly on the homogeneity of the selenized films. Cracks in the spray-deposited films resulted in uneven selenization rates and sintering by creating paths for rapid, uncontrollable selenium (Se) vapor penetration. To make crack-free films, the nanocrystals had to be completely coated with capping ligands in the ink. The selenization rate of crack-free films then depended on the thickness of the nanocrystal layer, the temperature, and duration of Se vapor exposure. Either inadequate or excessive Se exposure leads to poor device performance, generating films that were either partially sintered or exhibited significant accumulation of selenium. The deposition of uniform nanocrystal films is expected to be important for a variety of electronic and optoelectronic device applications.

**Keywords:** Photovoltaics, Nanocrystals, Selenization, CIGS, Copper Indium Gallium Selenide

## Introduction

Colloidal nanocrystals are potentially useful for many emerging applications because of their wide range of unique, size-tunable properties.[1–5] These applications often require nanocrystals deposited on a substrate. Since nanocrystals are typically coated with capping ligands and dispersible in a variety of solvents, they can be deposited using solution-based printing schemes.[6] After deposition, the capping ligands tend to limit the electrical conductivity of the nanocrystal layers and must be removed, either by capping ligand exchange or stripping,[7–9] or by fusing the nanocrystals by heating.[6,10–14] These processes have enabled high mobility thin film transistors (TFTs),[5,15,16] high efficiency light-emitting diodes (LEDs),[17–20] photodetectors,[21] and photovoltaic devices (PVs).[3,8,12,22–24]

For PVs, a variety of different nanocrystals have been explored, including PbS,[8] $CuInSe_2$,[25,26] Cu(In,Ga)$Se_2$ (CIGS),[11,12,14] $CsPbI_3$,[27,28] $Cu_2ZnSnS_4$ (CZTS),[29–31] CdSe,[32] and CdTe.[13,33] Ligand exchange strategies have enabled devices with power conversion efficiencies (PCEs) of just over 13%,[8,27] and sintered nanocrystal layers processed at high temperature ($300^{o}$C-$600^{o}$C) have been used to make devices with even higher efficiency (PCE>16%).[11–14] To ensure consistent ligand removal or sintering and limit shunting in the devices, the as-deposited nanocrystal films need to be uniform.[11] Uniformity is difficult to achieve in a single deposition step for relatively thick films (>200 nm), because of the tendency to form cracks and voids as the solvent evaporates from the deposited ink.[25,34] Spin coating has been commonly used to make smooth and continuous nanocrystal films, but this method is only suitable for relatively thin layers (<200 nm), and thicker films require multiple deposition steps.[13,35–37] Thick films without cracks have been demonstrated using controlled solvent evaporation[25] or layer-by-layer deposition strategies,[11,35,36,38–41] but these methods are too slow to be used for commercial device fabrication.[42] Here, we report the use of an automated ultrasonic spray process to rapidly produce uniform, relatively thick (>1 μm), crack-free nanocrystal films. This method enables deposition of the nanocrystal layer in a single step with a high degree of thickness uniformity over a large substrate area, which is especially useful for applications like PVs that require large device areas with very few macroscopic defects.

The materials and processing parameters necessary to deposit thick, crack-free films of colloidal CIGS nanocrystals with an automated spray process in a single processing step are detailed herein. The spray-deposited CIGS nanocrystal films were selenized by heating above 500$^{o}$C under selenium (Se) vapor, and incorporated into PVs. Cracks in the deposited layer led to large inhomogeneities in the selenized film and very poor device performance. We found that cracking could be prevented by ensuring that the nanocrystals had complete ligand coverage in the ink without a significant excess of free ligand. Using crack-free spray-deposited films, the selenization process could be controlled by adjusting the temperature and duration of Se exposure to obtain uniformly sintered films that performed well in PVs.

## Experimental Details

***Materials.*** Elemental Se powder (99.99%, 100 mesh), copper chloride (CuCl, 99.99+%), and cadmium sulfate ($CdSO_4$, 99.999%) were purchased from Aldrich Chemical Co. Ethanol (absolute), toluene (99.99%) and ammonium hydroxide ($NH_4OH$, 18 M; ACS certified) were purchased from Fisher Scientific. Thiourea ($CH_4N_2S$, >99.0%) was purchased from Sigma-Aldrich. Gallium chloride ($GaCl_3$, 99.999%) and indium chloride ($InCl_3$, 99.999%) were received from 5N Plus. Oleylamine ($C_{17}H_{37}N$, OLA, >70%) was purchased from TCI America.

***CIGS nanocrystal synthesis.*** CIGS nanocrystals were synthesized with a targeted composition of $CuIn_{0.65}Ga_{0.35}Se_2$ using published procedures.[11,25,43] Prior to use, OLA was degassed for 12 h at 110 °C under vacuum. In a three-neck flask in a $N_2$-filled glovebox, 4 mmol of CuCl (0.396 g), 2.6 mmol of $InCl_3$ (0.575 g), 1.4 mmol of $GaCl_3$ (0.247 g), and 8 mmol of Se (0.632 g) was combined with 30 mL of OLA. The flask was sealed with rubber septa, removed from the glovebox and attached to a Schlenk line. The mixture was placed under vacuum for 30 min at 110 °C and then blanketed with nitrogen. The temperature was increased at 12-14 °C/min to 240 °C. After 30 min, the heating mantel was removed and the reaction mixture was allowed to cool to room temperature. The nanocrystals were precipitated by adding 1-5 mL of ethanol to each g of reaction product and then centrifuging at an rcf of 2057 x g for 2 min in a 4.5 inch radius centrifuge (4000 rpm). The nanocrystals were redispersed in 10 mL of toluene and centrifuged to remove poorly capped nanocrystals. The supernatant was isolated and combined with 10 mL of ethanol and centrifuged to reprecipitate the nanocrystals. The nanocrystals were finally dispersed in toluene to a concentration of 10 mg/mL. This procedure yields approximately 200 mg of OLA-capped nanocrystals with diameters ranging between 8-20 nm, and a composition of $Cu_{0.78}In_{0.63}Ga_{0.25}Se_2$, as determined by energy-dispersive X-ray spectroscopy (EDS) on an FEI Quanta 650 FEG scanning electron microscope (SEM) with a Bruker XFlash EDS Detector 5010.

***PV device fabrication.*** PVs were fabricated on soda-lime glass with a glass/Mo/CIGS/CdS/ZnO/ITO stack.[11,43] Soda-lime glass (Delta Technology) substrates (25 mm x 25 mm) were sonicated in 1:1 vol/vol acetone/isopropanol, rinsed with deionized (DI) water, sonicated again in DI-$H_2O$, and dried with nitrogen. Mo was deposited with 1 μm thickness on by rf sputtering from a Mo target (Lesker, 99.95%) in two steps. After depositing 400 nm of an adhesive layer at 5 mTorr, the remainder of the Mo layer with higher conductivity was deposited at 1.5 mTorr.[44] Nanocrystals were deposited using a Sono-Tek ExactaCoat ultrasonic automated spray system with a 120 kHz ultrasonic nozzle onto substrates heated to 100 °C using a liquid flow rate of 0.275 mL/min and a nozzle air pressure of 2.6 psi (17.9 kPa). The nozzle was positioned 11.5 cm above the substrate and raster scanned with 3 mm spacing at a speed of 14 mm/s. Prior to selenization, the nanocrystal films were heated for 1 h at 525 °C under Ar in a Thermolyne 79500 tube furnace and then soaked in 1M NaCl solution for 10 min.[11,38] The substrates were then transferred into a nitrogen-filled glovebox and placed above a quartz boat filled with Se in a hollow graphite cylinder.[11,43] The cylinder was sealed, removed from the glove box and placed in the tube furnace under Ar and heated at 80 °C/min to 500°C for 10 min.[11,43]

A CdS buffer layer (50 nm) was deposited on the selenized nanocrystal film by chemical bath deposition (CBD). A 300 mL crystallization dish was filled with 160 mL DI-$H_2O$ and heated to 80 °C. After the temperature stabilizes, 25 mL of 15 mM $CdSO_4$, 12.5 mL of 1.5 M thiourea, and 32 mL of 18 M $NH_4OH$[45] were added to the dish followed by immediate immersion of the substrates in the bath for 15 min. The substrates were then rinsed with DI-$H_2O$ and dried with nitrogen. Finally, 50 nm of ZnO (99.9%, Lesker) and 600 nm indium tin oxide (ITO, 99.99%, Lesker) were sputter-deposited using an Angstrom Engineering AMOD at 2 mTorr through shadow masks to create an active area of 10 $mm^2$. The ITO was patterned with silver paint (SPI Supplies) grid lines. All devices were heated for 2 h at 225 °C in air at 1 atm prior to testing.

***Materials and Device Characterization.*** SEM images were obtained using a Zeiss Supra 40 VP SEM operated at 5 kV. Nanocrystal films that had not been selenized were imaged on Si wafer substrates. Thermogravimetric analysis (TGA) was carried out using a Mettler-Toledo DSC/TGA with 1 mg of nanocrystals heated at 10 °C/min. Current-voltage (IV) characteristics of the PVs were measured using a Keithley 2400 source meter under AM1.5G light from a Newport 91160 solar simulator tuned to 100 mW/cm$^2$ using a NIST calibrated Si photodiode (Hamamatsu, S1787-08). External quantum efficiency (EQE) measurements were obtained as previously described using a home-built instrument.[11]

## Results and Discussion

***Uniform Crack-Free Films of CIGS Nanocrystals.*** Figure 1 shows top and cross-section SEM views of a 1.3 μm layer of CIGS nanocrystals that was deposited using a fully automatic Sono-Tek ExactaCoat system with a 3-axis robotic arm. The film has uniform thickness and is free of cracks. Much of our previous PV fabrication research has utilized a pressure-driven hand sprayer to deposit CIGS nanocrystals.[11,43] The automated ultrasonic spray deposition process enables a much higher level of control and repeatability, producing a much more consistent droplet size of about 13 μm in diameter.[46] The thickness of the deposited films was found to depend on the concentration of the nanocrystals in the ink, the air pressure, liquid flow rate, raster line spacing, raster speed, and nozzle height; the roughness and morphology on the delivery rate of the nanocrystals to the surface, which is controlled by the liquid flow rate, ink concentration, nozzle height and nanocrystal concentration in the ink; and the amount of cracking in the film, by the way the nanocrystals were purified prior to dispersion in the ink.

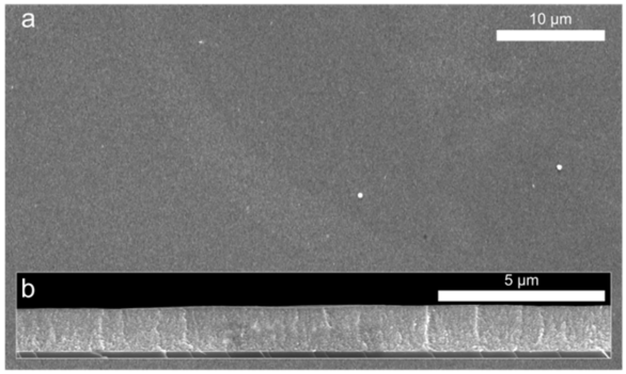


**Figure 1.** (a) Top-view and (b) cross-section SEM images of a uniform crack-free film of CIGS nanocrystals deposited using an ultrasonic spray process.

Figure 2 outlines the purification process used to isolate the nanocrystals from the reaction mixture and shows SEM images of two spray-deposited films—one with significant cracking and one without. Nanocrystal films with cracks had a visually matte appearance and those without cracks were shiny and optically reflective (Figures 2d and 2e). Both films in Figure 2 were deposited using the same spray parameters with similar nanocrystal concentrations in the ink. The only difference between the two films was in the way the nanocrystals were purified. The nanocrystals used to make the film with cracks were isolated from the reaction mixture with a relatively large amount of ethanol in the first purification step. We found that films exhibited significant cracking when nanocrystals were precipitated with more than 2.0 mL of ethanol/g of reaction product. Antisolvent precipitation is commonly used to purify nanocrystals[47,48] and known to strip ligands from the nanocrystal surface in many cases.[49-52] TGA of the CIGS nanocrystals showed that OLA ligand coverage was significantly affected by the amount of ethanol used in the purification step. In Figure 3, the weight loss event near 200°C corresponds to the loss of OLA from the sample and the total weight loss from the sample provides a measure of the amount of ligand coverage on the nanocrystals. One thing to note from the TGA data is that a relatively small difference in ligand coverage determines whether the spray-deposited film ends up with cracks. For example, nanocrystals precipitated with 3.0 mL or 1.5 mL of ethanol per g of reaction product are composed of 14 wt% or 18 wt% OLA, respectively. This is within the range expected for monolayer coverage of OLA on the nanocrystals.[53]

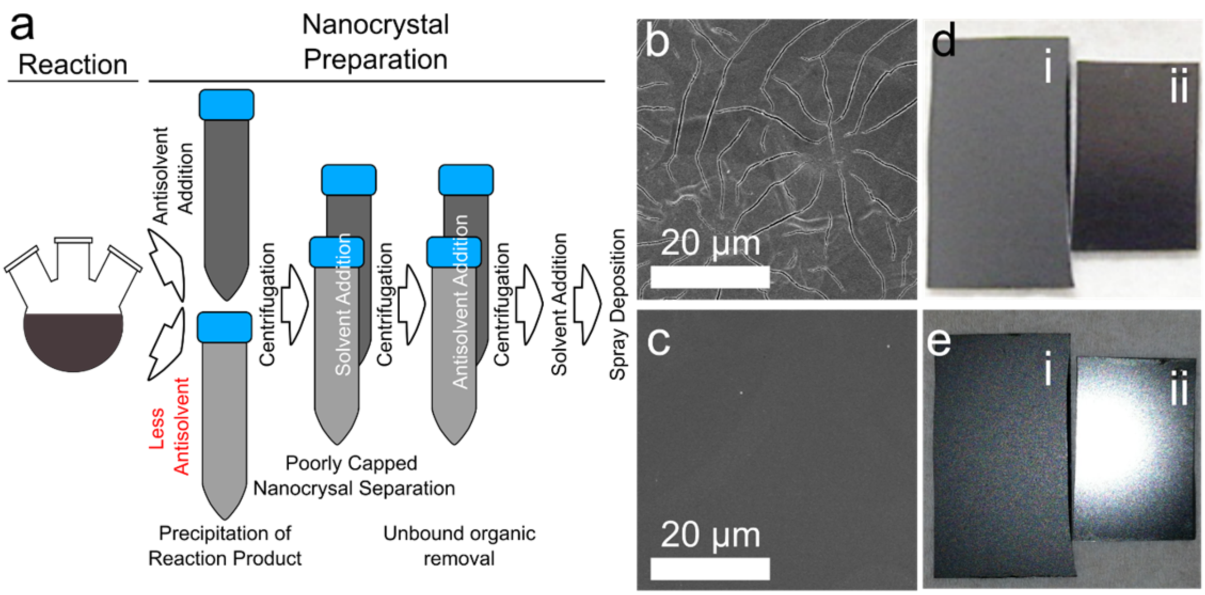


**Figure 2.** (a) The purification of CIGS nanocrystals is achieved by antisolvent precipitation using toluene and ethanol as the solvent:antisolvent pair. (b,c) SEM images of CIGS nanocrystal films with nanocrystals precipitated using (b) 3.0 mL and (c) 1.5 mL of ethanol/g reaction product. (d,e) Photos of the films in (b) and (c) taken (i) with and (ii) without a flash.

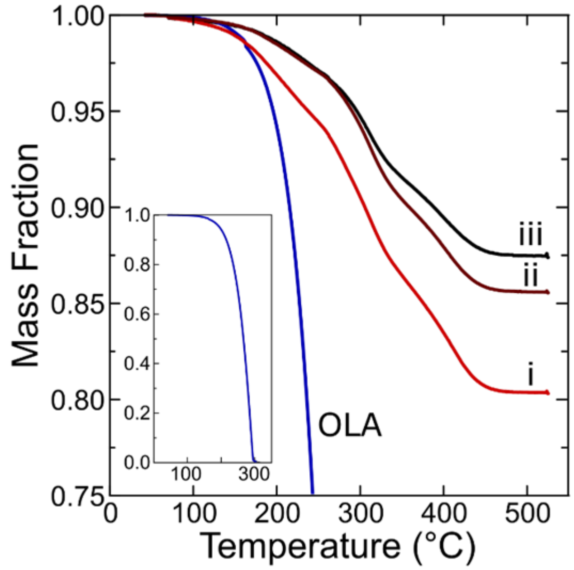


Figure 3. TGA of OLA-capped CIGS nanocrystals precipitated with 1.5 mL ethanol/g reaction product (i, red line), 3.0 mL anti-solvent/g reaction product (ii, brown line), and 4.5 mL anti-solvent/g reaction product (iii, black line). SEM images of the films made with the nanocrystals from trace i and trace ii are presented in Figures 2c and 2b, respectively. Inset: TGA of pure OLA.

Since the extent of OLA ligand coverage on the CIGS nanocrystals appeared to underlie the formation of cracks in the spray-deposited films, we tried to add OLA to OLA-poor nanocrystal inks prior to spray coating. As an example, nanocrystals that had been purified by adding 3 mL of ethanol per g of reaction product (which would form cracks when spray-deposited) were dispersed in toluene at a concentration of 10 mg/mL with additional OLA in amounts ranging between 0.25 vol% to 0.5 vol%, which corresponds to 1.5-3.0 eq. of OLA relative to the amount of OLA needed to provide monolayer coverage. There is sufficient OLA to achieve full ligand coverage; however, this post-purification addition of OLA to the nanocrystal ink did not alleviate the cracking of the deposited films. There is some reduction in the amount of cracking, but cracks are still observed, as in Figure 4b. In fact, the addition of OLA was problematic because excess OLA segregated from the nanocrystal film and created a residue on the surface, as in Figure 4c. Based on the observed cracking, it appears that the OLA added to the dispersion after the purification step is not incorporating into the capping ligand layer as necessary to eliminate crack formation. OLA residue also creates a major problem during the fabrication of PVs. Prior to selenization, the CIGS nanocrystal film are heated in Ar at 525°C for 1 hr to remove OLA from the layer, otherwise a thick carbon layer ends up forming that leads to poor device performance.[11] When OLA was added to the ink after purification, the pre-selenization anneal generated a significant concentration of holes in the film. The addition of OLA to the nanocrystal ink after purification could not be used to produce usable, crack-free films.

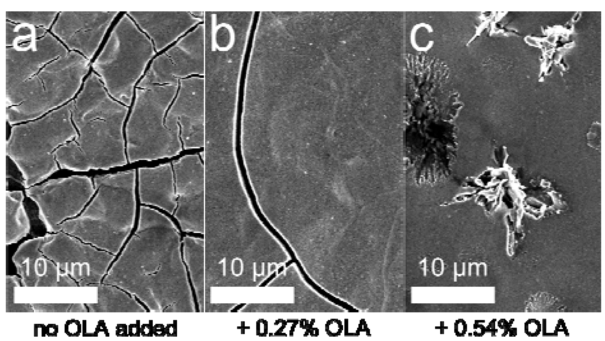


**Figure 4.** SEM images of CIGS nanocrystal films deposited with a) no added OLA, b) 0.27 vol% added OLA, and c) 0.54 vol% added OLA. Crack formation was reduced by the addition of OLA to the ink, but excess OLA was found to segregate to the nanocrystal surface.

These results show that adsorbed ligand plays a direct role in preventing cracks in the dried nanocrystal films and that it is not possible to simply add more free ligand to the ink to prevent cracking. This is because it is the weak attractive interactions between bonded capping ligands that pull the nanocrystals together and maintain the integrity of the film as the solvent evaporates. Cracks appear when the in-plane strain at the interface of the film created by the evaporation of residual solvent in the late stages of drying exceeds some limit of fracture toughness. Without capping ligands on the nanocrystals, there is only weak van der Waals attraction between the inorganic cores holding the particle film together to resist cracking. Kramer et al.[52] proposed that higher ligand coverage on nanocrystals can increase the toughness of a dried nanocrystal film and reduce the likelihood of crack formation during the drying process, by enhancing the interparticle attraction and strengthening the ligand-ligand interactions by interdigitation and tangling between ligands on neighboring nanocrystals.[54] Additional free ligand in the dried film does not play the same role because the ligand is not attached to the core of the nanocrystals and does not provide a robust link needed to significantly enhance the interparticle attractions or influence the integrity of the nanocrystal film.

***Cracks Influence the Selenization of CIGS nanocrystal films.*** The spray-deposited CIGS nanocrystal films were selenized and incorporated into PVs. Figure 5 shows SEM images of spray-deposited CIGS nanocrystal films before and after selenization. The crack-free film in Figures 5a, 5b, 5e and 5f has selenized uniformly, although in this particular film only the top layer of the nanocrystals have been sintered. As shown in Figures 5c, 5d, 5g and 5h, selenization of the film with cracks led to large (>5 μm) islands of sintered CIGS crystals on top of a more continuous sintered polycrystalline CIGS layer. The cracks appear to provide a path for Se vapor to penetrate deep into the film, even under it, leading to uneven recrystallization and grain growth, as illustrated in Figure 6. This leads to the observed islanding and disconnected selenized film morphologies in Figures 5g and 5h. Devices made from selenized films that had cracks exhibited little or no photoresponse.

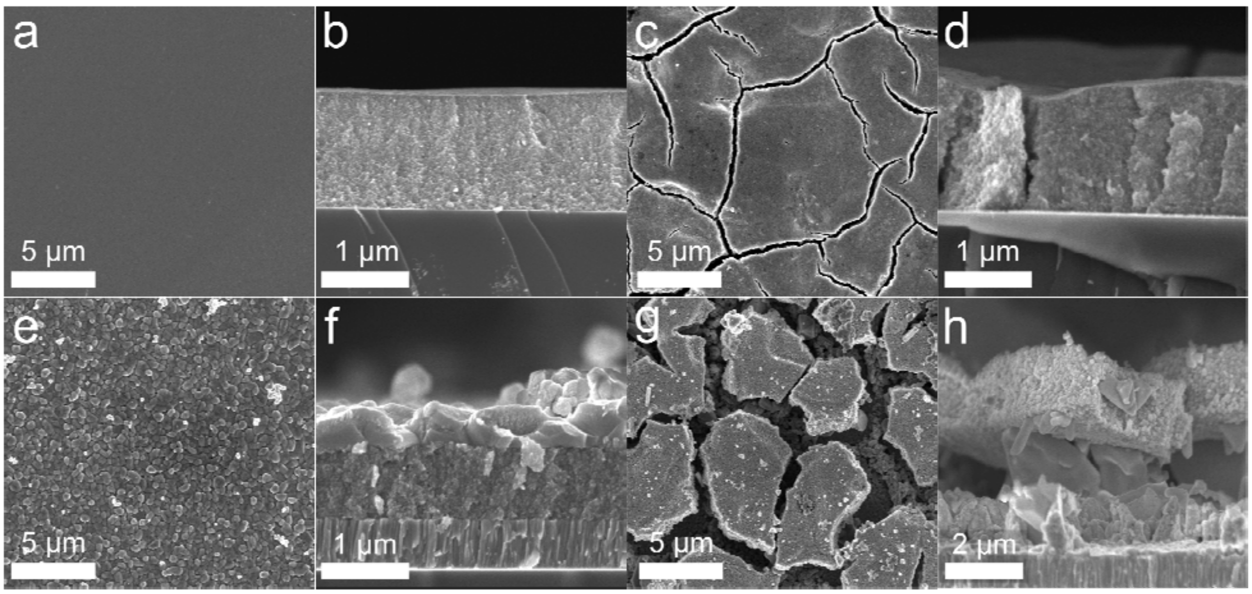


Figure 5: Spatial (a,c,e,g) and cross sectional (b,d,f,h) SEM images of films before (a-d) and after (e-h) selenization. The reflective film (a,b,e,f) is highly uniform after selenization, while matte films (c,d,g,h) become more heterogeneous.

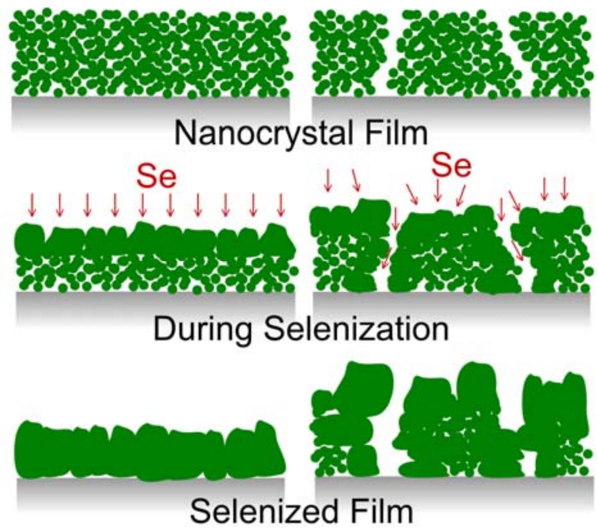


Figure 6: Selenization of nanocrystal films without cracks (left) and with cracks (right). In the crack-free films, Se evenly interacts with the nanocrystals and grain growth occurs evenly across the film. In the nanocrystal films with cracks, grain growth occurs at all exposed surfaces, leading to very uneven grain growth.

The power conversion efficiency (PCE) of PVs made from glossy, crack-free films depended on the selenization conditions and the initial nanocrystal film thickness. SEM images of two CIGS nanocrystal films deposited without cracks with different thickness, of 0.9 μm and 1.2 μm, are shown in Figure 7 after 10 min of exposure to Se vapor at 500°C or 550°C. Both films are not fully sintered after heating at 500°C. At the higher selenization temperature of 550°C, both films have completely sintered. A carbon-rich amorphous layer underlies both films. We have previously reported X-ray photoelectron spectroscopy (XPS) analysis of this layer, showing that is comprised of both Se and carbon[43] and can be eliminated by annealing the film in Ar before selenization.[11] One drawback of the crack-free films appears to be that it is more difficult to remove the excess carbon in the film before selenization. This becomes a problem especially when the selenization is carried out for too long and additional Se accumulates in this underlying carbon-rich layer.

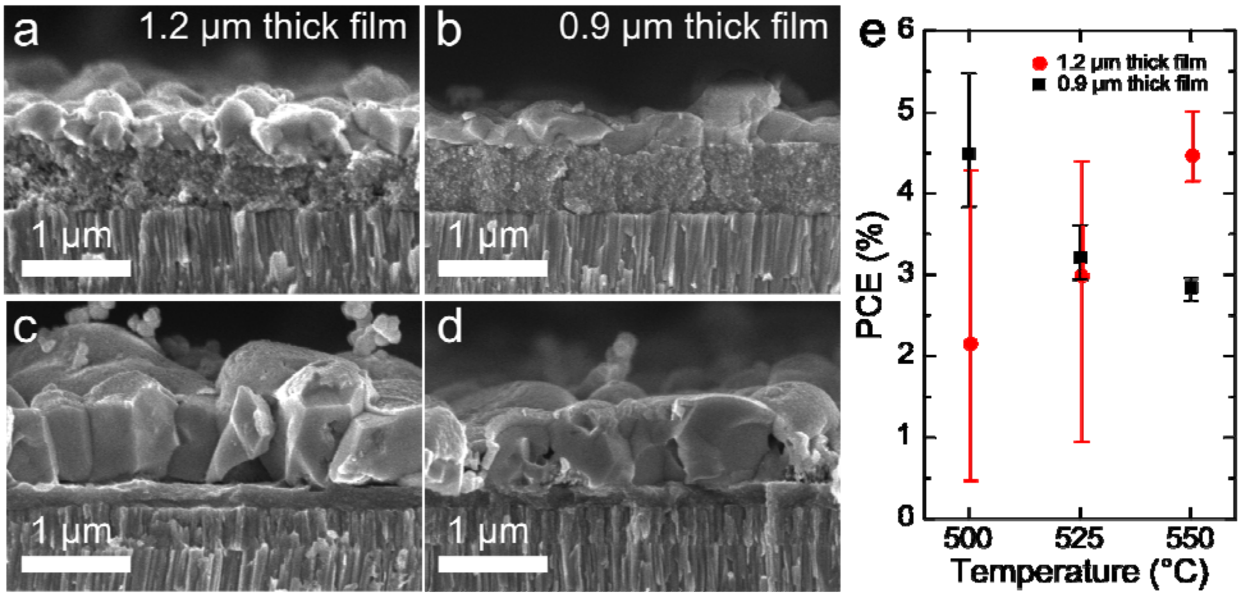


Figure 7: SEM images of $Cu(In,Ga)Se_2$ nanocrystal films with two thicknesses of (a,c) 1.2 µm and (b,d) 0.9 µm after 10 min of exposure to Se vapor at two different temperatures, of (a,b) 500°C and (c,b) 550°C. e) Average PCE of four devices fabricated from 1.2 µm (red circles) and 0.9 µm (black squares) nanocrystal films are exposed to Se vapor at 500°C, 525°C, and 550 °C for 10 min. The error bars indicate the highest and lowest PCEs of the four devices fabricated for each experimental condition.

The average PCE values of CIGS nanocrystal film PVs that were selenized for 10 min at 500°C, 525°C, or 550°C are shown in Figure 7e. The efficiency of devices made with 1.2 µm films improved with increased selenization temperature, while the opposite was true for devices fabricated with the thinner 0.9 µm films. This is because the thinner films become completely selenized at lower temperature than the thicker films. For these thinner films, the higher selenization temperature leads to an accumulation of Se in the device layer, particularly in the carbon-rich layer between the CIGS film and the Mo back contact, that deteriorates performance. This carbon-rich layer is known to be a challenge facing the fabrication of high efficiency CIGS PVs with nanocrystal inks.[55] For the thicker films, higher selenization temperatures are required to fully sinter the layer. One additional point is that the variability in performance of PVs made with thinner 0.9 μm CIGS layers was less than for the PVs with the thicker film for all selenization temperatures.

Figure 8 shows SEM images of a crack-free, 1.0 μm CIGS nanocrystal film before and after selenization at 550 °C for 10 min and the IV and EQE characteristics of the PV made with this layer. The device exhibits a PCE of 6.6%. The optimized parameters that were used to process this device were relatively reliable. For example, we made 12 devices over a two-week period and of these, 11 had non-linear JV response and were classified as non-shorted. These 11 functioning devices exhibited an average PCE=5.27%, $V_{oc}$=0.41 V, $J_{sc}$=25.8 $cm^2$, and FF=0.49. The fill factor was found to be the most variable device parameter. This probably relates to the difficulty in achieving good device performance when the nanocrystal layer changes significantly during the selenization process. For example, the nanocrystal films imaged in Figures 8a and 8b has shrunk from 1 μm to 350 nm after selenization. This thickness reduction can often lead to pinholes that reduce the fill factor and $V_{oc}$, and remains one of the primary challenges to achieving high efficiencies in selenized $Cu(In,Ga)Se_2$ nanocrystal films. One way to avoid the volume reduction is to selenize $Cu(In,Ga)S_2$ nanocrystals.[56]

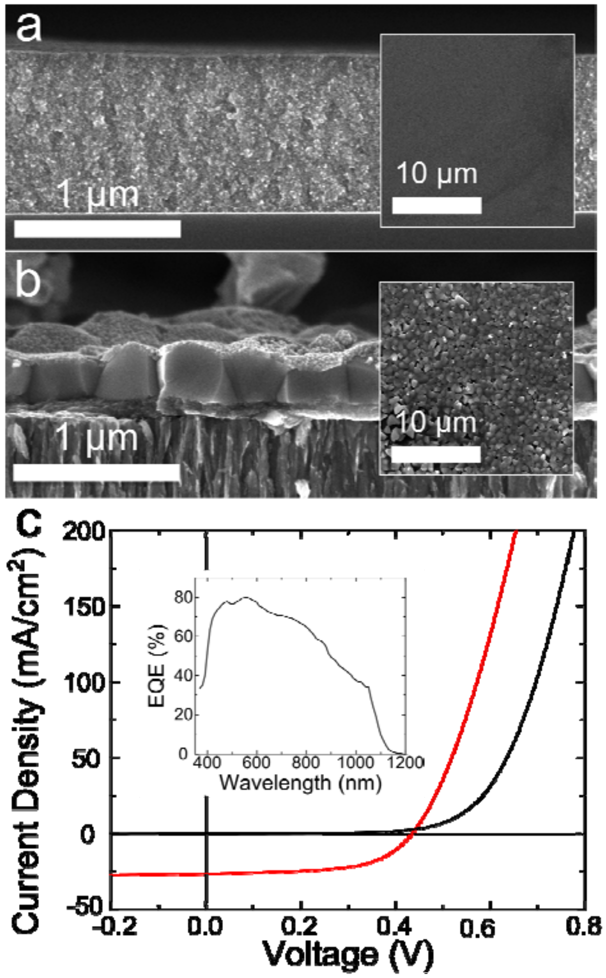


Figure 8. SEM images (spatial SEM inset) of $Cu_{0.78}In_{0.63}Ga_{0.25}Se_2$ nanocrystal films (a) before and (b) after selenization (10 min, 550°C). The insets in (a) and (b) are top-view SEM images of the layers. The images in (b) were acquired deposition of the CdS buffer layer. (c) Current-voltage response of the PV device fabricated with the selenized layer (PCE=6.6%, $J_{sc}$=26.3 mA/cm2, $V_{oc}$=0.43 V, and FF=0.59 under AM1.5, 100 mW/$cm^2$ conditions). The inset in (c) shows the EQE response of the device. The value of $J_{sc}$ calculated from the EQE data is 26.1 mA/$cm^2$, which is close to the measured $J_{sc}$.

## Conclusions

An automated ultrasonic spray deposition method was developed to deposit thick (>1 μm) layers of CIGS nanocrystals with uniform thickness and no cracks. It was crucial to have adequate OLA ligand capping to eliminate cracking in the films. When too much antisolvent was used to isolate the nanocrystals from the crude reaction product, the nanocrystal layers ended up having a significant amount of cracking. This was due to the loss of capping ligands during the purification process. It was not possible to simply add more OLA to the nanocrystal dispersion prior to the deposition to prevent cracks. Only OLA adsorbed on the nanocrystals helped to prevent cracks. The crack-free films enabled optimization of the selenization process to achieve reliable fabrication of devices with reasonably high efficiency. This work shows how subtle changes in nanocrystal purification and ink formulation can lead to significant differences in film morphology and properties, especially when relatively thick layers of nanocrystals are needed on large areas of substrate, as in the case especially of PVs.

**Acknowledgements**

We acknowledge funding of this research by the National Science Foundation Industry/University Cooperative Research Center for Next Generation Photovoltaics (grant no. IIP-1540028, IIP-1822206 and IIP-1624539) and the Robert A. Welch Foundation (grant no. F-1464). CJS and DRP also acknowledge support for this work by the National Science Foundation Graduate Research Fellowship under Grant No. DGE-1110007. FPB is grateful to Universidad Nacional de Córdoba for the exchange scholarship.

**References**

(1) Talapin, D. V.; Shevchenko, E. V. Introduction: Nanoparticle Chemistry. *Chem. Rev.* **2016**, *116*, 10343–10345.

(2) Kershaw, S. V.; Jing, L.; Huang, X.; Gao, M.; Rogach, A. L. Materials Aspects of Semiconductor Nanocrystals for Optoelectronic Applications. *Mater. Horizons* **2017**, *4*, 155–205.

(3) Stolle, C. J.; Harvey, T. B.; Korgel, B. A. Nanocrystal Photovoltaics: A Review of Recent Progress. *Curr. Opin. Chem. Eng.* **2013**, *2*, 160–167.

(4) Panthani, M. G.; Korgel, B. A. Nanocrystals for Electronics. *Annu. Rev. Chem. Biomol. Eng.* **2012**, *3*, 287–311.

(5) Zhu, J.; Hersam, M. C. Assembly and Electronic Applications of Colloidal Nanomaterials. *Adv. Mater.* **2017**, *29*, 1603895.

(6) Ridley, B. A.; Nivi, B.; Jacobson, J. M. All-Inorganic Field Effect Transistors Fabricated by Printing. *Science* **1999**, *286*, 746-749.

(7) Nag, A.; Kovalenko, M. V.; Lee, J.-S.; Liu, W.; Spokoyny, B.; Talapin, D. V. Metal-Free Inorganic Ligands for Colloidal Nanocrystals: $S^{2-}$, $HS^{-}$, $Se^{2-}$, $HSe^{-}$, $Te^{2-}$, $HTe^{-}$, $TeS_3^{2-}$, $OH^{-}$, and $NH_2^{-}$ as Surface Ligands. *J. Am. Chem. Soc.* **2011**, 133, 10612-10620.

(8) Liu, M.; Voznyy, O.; Sabatini, R.; Arquer, F. P. G. de; Munir, R.; Balawi, A. H.; Lan, X.; Fan, F.; Walters, G.; Kirmani, A. R.; Hoogland, S.; Laquai, F.; Amassian, A.; Sargent, E. H. Hybrid Organic–Inorganic Inks Flatten the Energy Landscape in Colloidal Quantum Dot Solids. *Nature Mater.* **2017**, *16*, 258–263.

(9) Stolle, C. J.; Panthani, M. G.; Harvey, T. B.; Akhavan, V. A.; Korgel, B. A. Comparison of the Photovoltaic Response of Oleylamine and Inorganic Ligand-Capped $CuInSe_2$ Nanocrystals. *ACS Appl. Mater. Interfaces* **2012**, *4*, 2757–2761.

(10) Stolle, C. J.; Harvey, T. B.; Pernik, D. R.; Hibbert, J. I.; Du, J.; Rhee, D. J.; Akhavan, V. A.; Schaller, R. D.; Korgel, B. A. Multiexciton Solar Cells of $CuInSe_2$ Nanocrystals. *J. Phys. Chem. Lett.* **2013**, *5*, 304–309.

(11) Harvey, T. B.; Mori, I.; Stolle, C. J.; Bogart, T. D.; Ostrowski, D. P.; Glaz, M. S.; Du, J.; Pernik, D. R.; Akhavan, V. A.; Kesrouani, H.; Vanden Bout, D. A.; Korgel, B. A. Copper Indium Gallium Selenide (CIGS) Photovoltaic Devices Made Using Multistep Selenization of Nanocrystal Films. *ACS Appl. Mater. Interfaces* **2013**, *5*, 9134–9140.

(12) McLeod, S. M.; Hages, C. J.; Carter, N. J.; Agrawal, R. Synthesis and Characterization of 15% Efficient CIGSSe Solar Cells from Nanoparticle Inks. *Prog. Photovoltaics: Res. Appl.* **2015**, *23*, 1550–1556.

(13) Crisp, R. W.; Panthani, M. G.; Rance, W. L.; Duenow, J. N.; Parilla, P. A.; Callahan, R.; Dabney, M. S.; Berry, J. J.; Talapin, D. V.; Luther, J. M. Nanocrystal Grain Growth and Device Architectures for High-Efficiency CdTe Ink-Based Photovoltaics. *ACS Nano* **2014**, *8*, 9063–9072.

(14) Eeles, A.; Arnou, P.; Bowers, J. W.; Walls, J. M.; Whitelegg, S.; Kirkham, P.; Allen, C.; Stubbs, S.; Liu, Z.; Masala, O.; Newman, C.; Pickett, N. High-Efficiency Nanoparticle Solution-Processed $Cu(In,Ga)(S,Se)_2$ Solar Cells. *IEEE J. Photovoltaics* **2018**, *8*, 288–292.

(15) Jang, J.; Dolzhnikov, D. S.; Liu, W.; Nam, S.; Shim, M.; Talapin, D. V. Solution-Processed Transistors Using Colloidal Nanocrystals with Composition-Matched Molecular “Solders”: Approaching Single Crystal Mobility. *Nano Lett.* **2015**, *15*, 6309–6317.

(16) Talapin, D. V.; Murray, C. B. PbSe Nanocrystal Solids for N- and p-Channel Thin Film Field-Effect Transistors. *Science* **2005**, *310*, 86–89.

(17) Mastria, R.; Rizzo, A. Mastering Heterostructured Colloidal Nanocrystal Properties for Light-Emitting Diodes and Solar Cells. *J. Mater. Chem. C* **2016**, *4*, 6430–6446.

(18) Gong, X.; Yang, Z.; Walters, G.; Comin, R.; Ning, Z.; Beauregard, E.; Adinolfi, V.; Voznyy, O.; Sargent, E. H. Highly Efficient Quantum Dot Near-Infrared Light-Emitting Diodes. *Nature Photonics* **2016**, *10*, 253–257.

(19) Supran, G. J.; Song, K. W.; Hwang, G. W.; Correa, R. E.; Scherer, J.; Dauler, E. A.; Shirasaki, Y.; Bawendi, M. G.; Bulović, V. High-Performance Shortwave-Infrared Light-Emitting Devices Using Core–Shell (PbS–CdS) Colloidal Quantum Dots. *Adv. Mater.* **2015**, *27*, 1437–1442.

(20) Li, X.; Zhao, Y.-B.; Fan, F.; Levina, L.; Liu, M.; Quintero-Bermudez, R.; Gong, X.; Quan, L. N.; Fan, J.; Yang, Z.; Hoogland, S.; Voznyy, O.; Lu, Z.-H.; Sargent, E. H. Bright Colloidal Quantum Dot Light-Emitting Diodes Enabled by Efficient Chlorination. *Nat. Photon.* **2018**, *12*, 159–164.

(21) Arquer, F. P. G. de; Armin, A.; Meredith, P.; Sargent, E. H. Solution-Processed Semiconductors for next-Generation Photodetectors. *Nature Rev. Mater.* **2017**, *2*, 16100.

(22) Stroyuk, O.; Raevskaya, A.; Gaponik, N. Solar Light Harvesting with Multinary Metal Chalcogenide Nanocrystals. *Chem. Soc. Rev.* **2018**, *47*, 5354–5422.

(23) Semonin, O. E.; Luther, J. M.; Choi, S.; Chen, H.-Y.; Gao, J.; Nozik, A. J.; Beard, M. C. Peak External Photocurrent Quantum Efficiency Exceeding 100% via MEG in a Quantum Dot Solar Cell. *Science* **2011**, *334*, 1530–1533.

(24) Voggu, V. R.; Sham, J.; Pfeffer, S.; Pate, J.; Fillip, L.; Harvey, T. B.; Brown, R. M.; Korgel, B. A. Flexible $CuInSe_2$ Nanocrystal Solar Cells on Paper. *ACS Energy Lett.* **2017**, *2*, 574–581.

(25) Panthani, M. G.; Akhavan, V.; Goodfellow, B.; Schmidtke, J. P.; Dunn, L.; Dodabalapur, A.; Barbara, P. F.; Korgel, B. A. Synthesis of $CuInS_2$, $CuInSe_2$, and $Cu(In_xGa_{1-x})Se_2$ (CIGS) Nanocrystal "Inks" for Printable Photovoltaics. *J. Am. Chem. Soc.* **2008**, *130*, 16770–16777.

(26) Akhavan, V. A.; Goodfellow, B. W.; Panthani, M. G.; Steinhagen, C.; Harvey, T. B.; Stolle, C. J.; Korgel, B. A. Colloidal CIGS and CZTS Nanocrystals: A Precursor Route to Printed Photovoltaics. *J. Solid State Chem.* **2012**, *189*, 2–12.

(27) Sanehira, E. M.; Marshall, A. R.; Christians, J. A.; Harvey, S. P.; Ciesielski, P. N.; Wheeler, L. M.; Schulz, P.; Lin, L. Y.; Beard, M. C.; Luther, J. M. Enhanced Mobility $CsPbI_3$ Quantum Dot Arrays for Record-Efficiency, High-Voltage Photovoltaic Cells. *Sci. Adv.* **2017**, *3*, eaao4204.

(28) Wheeler, L. M.; Sanehira, E. M.; Marshall, A. R.; Schulz, P.; Suri, M.; Anderson, N. C.; Christians, J. A.; Nordlund, D.; Sokaras, D.; Kroll, T.; Harvey, S. P.; Berry, J. J.; Lin, L. Y.; Luther, J. M.Targeted Ligand-Exchange Chemistry on Cesium Lead Halide Perovskite Quantum Dots for High-Efficiency Photovoltaics. *J. Am. Chem. Soc.* **2018**, *140*, 10504–10513.

(29) Larramona, G.; Bourdais, S.; Jacob, A.; Choné, C.; Muto, T.; Cuccaro, Y.; Delatouche, B.; Moisan, C.; Péré, D.; Dennler, G. 8.6% Efficient CZTSSe Solar Cells Sprayed from Water–Ethanol CZTS Colloidal Solutions. *J. Phys. Chem. Lett.* **2014**, *5*, 3763–3767.

(30) Guo, Q.; Ford, G. M.; Yang, W.-C.; Walker, B. C.; Stach, E. A.; Hillhouse, H. W.; Agrawal, R. Fabrication of 7.2% Efficient CZTSSe Solar Cells Using CZTS Nanocrystals. *J. Am. Chem. Soc.* **2010**, *132*, 17384–17386.

(31) Steinhagen, C.; Panthani, M. G.; Akhavan, V.; Goodfellow, B.; Koo, B.; Korgel, B. A. Synthesis of $Cu_2ZnSnS_4$ Nanocrystals for Use in Low-Cost Photovoltaics. *J. Am. Chem. Soc.* **2009**, *131*, 12554–12555.

(32) Gur, I.; Fromer, N. A.; Geier, M. L.; Alivisatos, A. P. Air-Stable All-Inorganic Nanocrystal Solar Cells Processed from Solution. *Science* **2005**, *310*, 462–465.

(33) Panthani, M. G.; Kurley, J. M.; Crisp, R. W.; Dietz, T. C.; Ezzyat, T.; Luther, J. M.; Talapin, D. V. High Efficiency Solution Processed Sintered CdTe Nanocrystal Solar Cells: The Role of Interfaces. *Nano Lett.* **2013**, *14*, 670–675.

(34) Talapin, D. V.; Lee, J.-S.; Kovalenko, M. V.; Shevchenko, E. V. Prospects of Colloidal Nanocrystals for Electronic and Optoelectronic Applications. *Chem. Rev.* **2010**, *110*, 389–458.

(35) Todorov, T. K.; Gunawan, O.; Gokmen, T.; Mitzi, D. B. Solution-Processed Cu(In,Ga)$(S,Se)_2$ Absorber Yielding a 15.2% Efficient Solar Cell. *Prog. Photovoltaics* **2013**, *21*, 82–87.

(36) Cho, A.; Ahn, S.; Yun, J. H.; Gwak, J.; Song, H.; Yoon, K. A Hybrid Ink of Binary Copper Sulfide Nanoparticles and Indium Precursor Solution for a Dense $CuInSe_2$ Absorber Thin Film and Its Photovoltaic Performance. *J. Mater. Chem.* **2012**, *22*, 17893–17899.

(37) Xie, Y.; Chen, H.; Li, A.; Zhu, X.; Zhang, L.; Qin, M.; Wang, Y.; Liu, Y.; Huang, F. A Facile Molecular Precursor-Based Cu(In,Ga)$(S,Se)_2$ Solar Cell with 8.6% Efficiency. *J. Mater. Chem. A* **2014**, *2*, 13237–13240.

(38) Guo, Q.; Ford, G. M.; Agrawal, R.; Hillhouse, H. W. Ink Formulation and Low-Temperature Incorporation of Sodium to Yield 12% Efficient Cu(In,Ga)$(S,Se)_2$ Solar Cells from Sulfide Nanocrystal Inks. *Prog. Photovoltaics* **2013**, *21*, 64–71.

(39) Park, S.-W.; Kim, D.-I.; Lee, T.-S.; Lee, K.; Yoon, Y.; Cho, Y. H.; Kim, J. H.; Ahn, K. M.; Lee, K. J.; Jeon, C.-W. Solid-State Selenization of Printed Cu(In,Ga)$S_2$ Nanocrystal Layer and Its Impact on Solar Cell Performance. *Sol. Energy Mater. Sol. Cells* **2014**, *125*, 66–71.

(40) Cai, Y.; Ho, J. C. W.; Batabyal, S. K.; Liu, W.; Sun, Y.; Mhaisalkar, S. G.; Wong, L. H. Nanoparticle-Induced Grain Growth of Carbon-Free Solution-Processed CuIn$(S,Se)_2$ Solar Cell with 6% Efficiency. *ACS Appl. Mater. Interfaces* **2013**, *5*, 1533–1537.

(41) Swarnkar, A.; Marshall, A. R.; Sanehira, E. M.; Chernomordik, B. D.; Moore, D. T.; Christians, J. A.; Chakrabarti, T.; Luther, J. M. Quantum Dot–Induced Phase Stabilization of α-$CsPbI_3$ Perovskite for High-Efficiency Photovoltaics. *Science* **2016**, *354*, 92–95.

(42) Dhere, N. G. Scale-up Issues of CIGS Thin Film PV Modules. *Sol. Energy Mater. Sol. Cells* **2011**, *95*, 277–280.

(43) Akhavan, V. A.; Harvey, T. B.; Stolle, C. J.; Ostrowski, D. P.; Glaz, M. S.; Goodfellow, B. W.; Panthani, M. G.; Reid, D. K.; Vanden Bout, D. A.; Korgel, B. A. Influence of Composition on the Performance of Sintered Cu(In,Ga)$Se_2$ Nanocrystal Thin-Film Photovoltaic Devices. *ChemSusChem* **2013**, *6*, 481–486.

(44) Scofield, J. H.; Duda, A.; Albin, D.; Ballard, B. L.; Predecki, P. K. Sputtered Molybdenum Bilayer Back Contact for Copper Indium Diselenide-Based Polycrystalline Thin-Film Solar Cells. *Thin Solid Films* **1995**, *260*, 26–31.

(45) Hashimoto, Y.; Kohara, N.; Negami, T.; Nishitani, N.; Wada, T. Chemical Bath Deposition of Cds Buffer Layer for GIGS Solar Cells. *Sol. Energy Mater. Sol. Cells* **1998**, *50*, 71–77.

(46) How Ultrasonic Nozzles Work. *Sono-Tek*.

(47) Kowalczyk, B.; Lagzi, I.; Grzybowski, B. A. Nanoseparations: Strategies for Size and/or Shape-Selective Purification of Nanoparticles. *Curr. Opin. Colloid Interface Sci.* **2011**, *16*, 135–148.

(48) Murray, C. B.; Norris, D. J.; Bawendi, M. G. Synthesis and Characterization of Nearly Monodisperse CdE (E = Sulfur, Selenium, Tellurium) Semiconductor Nanocrystallites. *J. Am. Chem. Soc.* **1993**, *115*, 8706–8715.

(49) Goodwin, E. D.; Diroll, B. T.; Oh, S. J.; Paik, T.; Murray, C. B.; Kagan, C. R. Effects of Post-Synthesis Processing on CdSe Nanocrystals and Their Solids: Correlation between Surface Chemistry and Optoelectronic Properties. *J. Phys. Chem. C* **2014**, *118*, 27097–27105.

(50) Ip, A. H.; Thon, S. M.; Hoogland, S.; Voznyy, O.; Zhitomirsky, D.; Debnath, R.; Levina, L.; Rollny, L. R.; Carey, G. H.; Fischer, A.; Kemp, K. W.; Kramer, I. J.; Ning, Z.; Labelle, A. J.; Chou, K. W.; Amassian, A.; Sargent, E. H. Hybrid Passivated Colloidal Quantum Dot Solids. *Nat Nano* **2012**, *7*, 577–582.

(51) Choi, J. J.; Bealing, C. R.; Bian, K.; Hughes, K. J.; Zhang, W.; Smilgies, D.-M.; Hennig, R. G.; Engstrom, J. R.; Hanrath, T. Controlling Nanocrystal Superlattice Symmetry and Shape-Anisotropic Interactions through Variable Ligand Surface Coverage. *J. Am. Chem. Soc.* **2011**, *133*, 3131–3138.

(52) Kramer, T. J.; Kumar, S. K.; Steigerwald, M. L.; Herman, I. P. Reducing Strain and Fracture of Electrophoretically Deposited CdSe Nanocrystal Films. I. Postdeposition Infusion of Capping Ligands. *J. Phys. Chem. B* **2013**, *117*, 1537–1543.

(53) Dierick, R.; Van den Broeck, F.; De Nolf, K.; Zhao, Q.; Vantomme, A.; Martins, J. C.; Hens, Z. Surface Chemistry of $CuInS_2$ Colloidal Nanocrystals, Tight Binding of L-Type Ligands. *Chem. Mater*. **2014**, *26*, 5950–5957.

(54) Goodfellow, B. W.; Yu, Y.; Bosoy, C. A.; Smilgies, D.-M.; Korgel, B. A. The Role of Ligand Packing Frustration in Body-Centered Cubic (bcc) Superlattices of Colloidal Nanocrystals. *J. Phys. Chem. Lett.* **2015**, *6*, 2406-2412.

(55) Lee, D.; Yong, K. Non-Vacuum Deposition of CIGS Absorber Films for Low-Cost Thin Film Solar Cells. *Korean J. Chem. Eng.* **2013**, *30*, 1347-1358.

(56) Guo, Q.; Ford, G. M.; Hillhouse, H. W.; Agrawal, R. Sulfide Nanocrystal Inks for Dense $Cu(In_{1-x}Ga_x)(S_{1-y}Se_y)_2$ Absorber Films and Their Photovoltaic Performance. *Nano Lett.* **2009**, *9*, 3060–3065.

**For Table of Contents Use Only**

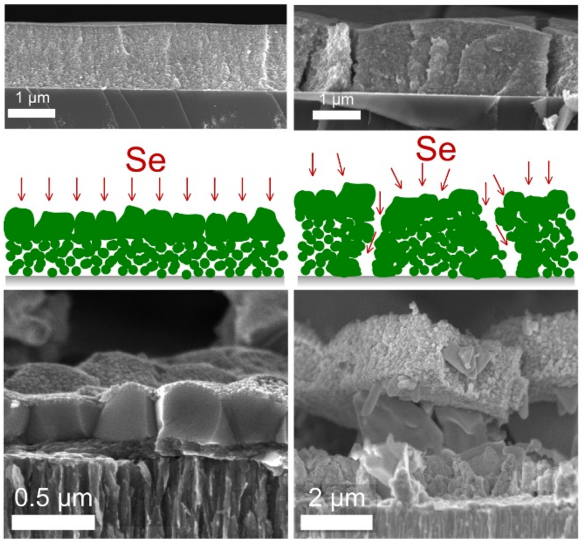
1 μm
1 μm
Se
Se
0.5 μm
2 μm